Preliminary Introduction of a Free Vortex Wake Method Into OpenFAST

K. Shaler[1], E. Branlard, A. Platt, and J. Jonkman
National Renewable Energy Laboratory, Golden, CO 80401, USA
E-mail: kelsey.shaler@nrel.gov

Abstract. Increasing wind turbine size can have substantial economic benefits. However, increasing wind turbine turbine size requires the use of models that accurately capture the aerodynamic response to large deflections and nonstraight blade geometries. Additionally, the installation of offshore floating turbines requires turbine models that can handle large rotor motion. Free vortex wake (FVW) methods are capable of modeling this type of complex physics while remaining computationally tractable to perform the many simulations necessary for turbine design. In this work, a FVW model is added to the National Renewable Energy Laboratory engineering tool OpenFAST to allow for the aerodynamic modeling of highly flexible turbines along with the aero-hydro-servo-elastic response capabilities of OpenFAST. Code implementation is not complete and thus no results are presented. However, areas of potential modeling improvement are discussed, such as modifications to the circulation calculation and the need for different FVW input model specifications when high-thrust cases are being modeled.

1. Introduction

Over the past few decades, substantial reductions in the cost of wind energy have come from large increases in rotor size. Larger rotors capture substantially more energy through greater swept area, yielding a reduced specific power while increasing turbine capacity factor. Research has shown that low specific power rotors, with correspondingly higher capacity factors, can lead to higher economic value [28]. One important consideration for such large turbines, however, is increased blade flexibility and the use of multielement airfoils (e.g., the use of flaps). In particular, large blade deflections may lead to a swept area that deviates significantly from the rotor plane. Such deviations violate assumptions used by common aerodynamic models, such as the blade element momentum (BEM) method, which rely on actuator-disk assumptions that are only valid for axisymmetric rotor loads contained in a plane. Large blade deflections may also cause the turbine near wake to diverge from a uniform helical shape. Further, interactions between turbine blades and the local near wake may increase, thus violating assumptions of models that do not account for the position and dynamics of the near wake. Additionally, highly flexible blades will likely cause increased unsteadiness and three-dimensionality of the aerodynamic effects, increasing the importance of accurate and robust

[1] Previous address: Department of Mechanical and Aerospace Engineering, Ohio State University, Columbus, OH.

dynamic stall models. There are many other complex wind turbine situations that violate simple engineering assumptions. Such situations include obtaining accurate aerodynamic loads for nonstraight blade geometries (e.g., built-in curvature or sweep); skewed flow caused by yawed inflow or turbine tilt; and large rotor motion as a result of placing the turbine atop a compliant floating platform offshore.

Higher-fidelity aerodynamic models are necessary to account for the increased complexity of flexible rotors. Although computational fluid dynamic (CFD) methods are able to capture such features, the computational cost limits the number of simulations that can be practically performed, which is an important consideration in load analysis for turbine design. Free vortex wake (FVW) methods are capable of modeling the complex physics, while remaining less computationally expensive than CFD methods. Numerous vorticity-based tools have been implemented, ranging from the early treatments by Rosenhead [19], the formulation of vortex particle methods by Winckelmans and Leonard [27], to the recent mixed Eulerian-Lagrangian compressible formulations of Papadakis [16]. Examples of long-standing codes that have been applied in the field of wind energy include GENUVP [25], using vortex particles methods, and AWSM [23], using vortex filament methods. Both tools have successively been coupled to structural solvers. The method was extended by Branlard et al. [6] to consistently use vortex methods to perform aero-elastic simulations of wind turbines in sheared and turbulent inflow. Most formulations rely on a lifting-line representation of the blades, but recently, a viscous-inviscid representation was also used in combination with a structural solver [21].

In this work, a FVW model is added to the National Renewable Energy Laboratory physics-based engineering tool OpenFAST, which solves the aero-hydro-servo-elastic dynamics of individual wind turbines. Incorporating the FVW model within OpenFAST allows for the modeling of highly flexible turbines along with the aero-hydro-servo-elastic response capabilities of OpenFAST. Code integration and modification are ongoing. Therefore, this work is considered a preliminary study to identify potential areas of improvement for the OpenFAST-FVW code.

2. Approach and Methods

This section details the FVW method and provides an overview of the computational method, followed by a brief explanation of its integration with OpenFAST.

2.1. Free Vortex Wake Model

This work employs a FVW method that solves for the turbine wake in a time-accurate manner, which allows the vortices to convect, stretch, and diffuse. The FVW model is based on a Lagrangian approach, in which the turbine wake is discretized into Lagrangian markers. The position of the Lagrangian markers is defined in terms of wake age, ζ, and azimuthal blade location, ψ. There are many methods of representing the wake with Lagrangian markers [5]. In this work, a hybrid lattice/filament method is used, as depicted in Figure 1. A lattice method is used in the near wake of the blade. The near wake spans over a user-specified angle. Though past research has indicated that a near-wake region of 30° is sufficient [14, 2], it was found in this work that a larger near wake is required for high thrust and other challenging conditions. After this period, the wake is assumed to instantaneously roll up into a tip vortex, which is assumed to be the most dominant feature for the remainder of the wake [15]. Each Lagrangian marker is connected to adjacent markers by straight-line vortex filaments, approximated to second-order accuracy [8]. The wake is initially assumed to be a helical wake and discretized ($d\psi$) based on turbine rotor speed (Ω) and a specified time step (dt), such that $d\psi = dt \times \Omega$. After this initial helical discretization, the wake is allowed to move and distort, thus changing the wake structure as the markers are convected downstream. To limit computational expense, the tip vortex is truncated after a specified number of rotor diameters (D) downstream of the turbine, which results in N wake revolutions. Because induced velocity information is a necessary boundary

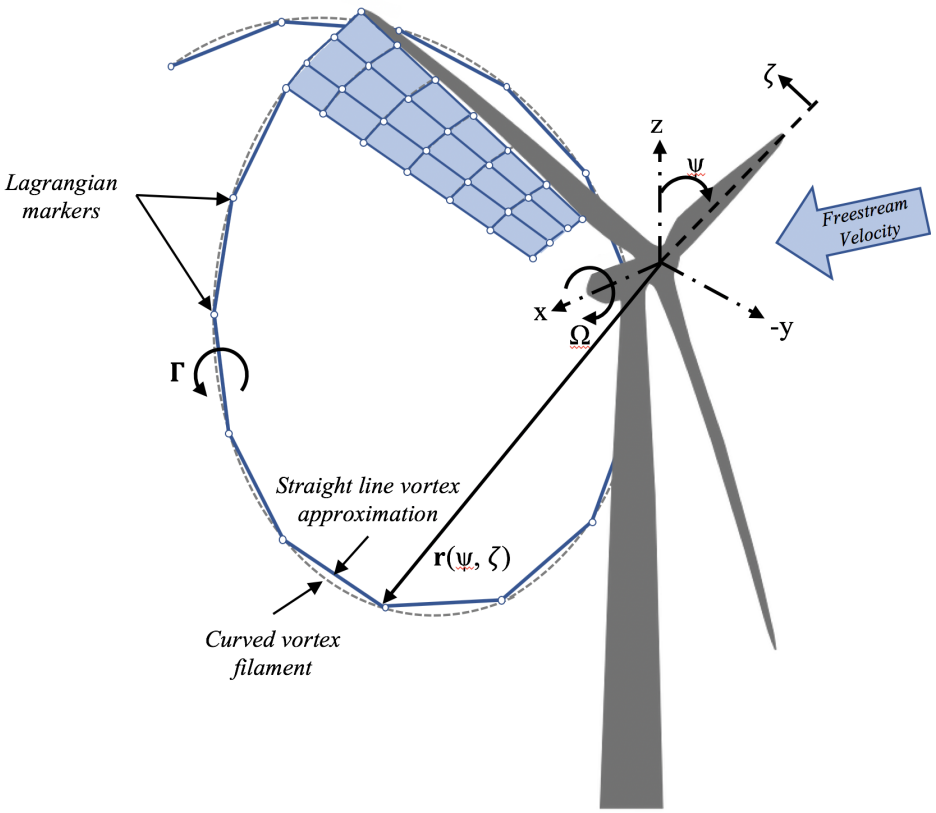

Figure 1. Evolution of near-wake lattice, blade tip vortex, and Lagrangian markers.

condition for wake truncation, an additional rotation $(N+1)$ is defined at the end of the wake and set to be identical to the previous N revolution. In this way, truncation error is minimized [15].

The governing equation of motion for a vortex filament is given by:

$$\frac{d\vec{r}(\psi,\zeta)}{dt} = \vec{V}[\vec{r}(\psi,\zeta),t] \tag{1}$$

Using the chain rule, Equation 1 is rewritten as:

$$\frac{\partial\vec{r}(\psi,\zeta)}{\partial\psi} + \frac{\partial\vec{r}(\psi,\zeta)}{\partial\zeta} = \frac{\vec{V}[\vec{r}(\psi,\zeta),t]}{\Omega} \tag{2}$$

where $d\psi/dt = \Omega$ and $d\psi = d\zeta$ [15]. Here, $\vec{r}(\psi,\zeta)$ is the position vector of a Lagrangian marker, and $\vec{V}[\vec{r}(\psi,\zeta)]$ is the velocity.

At present, a predictor-corrector scheme is used to numerically solve the left-hand side of Equation 2 for the vortex filament location. It was developed to accommodate variable rotor speed, as shown by the stencil in Figure 2 [22]. The difference operators $\frac{\partial\vec{r}(\psi,\zeta)}{\partial\zeta}$ and $\frac{\partial\vec{r}(\psi,\zeta)}{\partial\psi}$ are found by means of a Taylor series expansion about the point $(\zeta + \Delta\zeta/2,\ \psi + \Delta\psi/2)$. $\frac{\partial\vec{r}(\psi,\zeta)}{\partial\psi}$ is computed using a two steps backward method and $\frac{\partial\vec{r}(\psi,\zeta)}{\partial\zeta}$ by central differencing. This results in a scheme that is second-order accurate in ζ and third-order accurate in ψ. The resulting equations are given as follows:

$$\frac{\partial\vec{r}(\psi,\zeta)}{\partial\zeta} = \frac{\vec{r}(\psi+\Delta\psi_i,\zeta+\Delta\zeta) - \vec{r}(\psi+\Delta\psi_i,\zeta) + \vec{r}(\psi,\zeta+\Delta\zeta) - \vec{r}(\psi,\zeta)}{2\Delta\zeta} \tag{3}$$

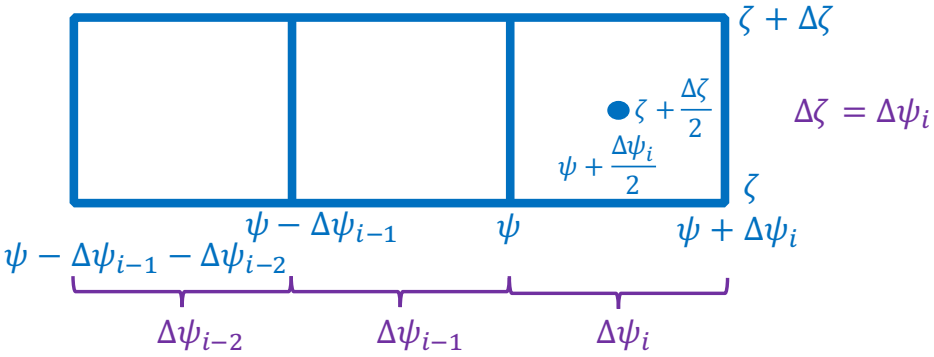

Figure 2. Variable rotor speed stencil used in time-marching predictor-corrector scheme.

$$\frac{\partial\vec{r}(\psi,\zeta)}{\partial\psi} = \Big\{23\vec{r}(\psi+\Delta\psi_i,\zeta+\Delta\zeta) + 23\vec{r}(\psi+\Delta\psi_i,\zeta) - 21\vec{r}(\psi,\zeta+\Delta\zeta) - 21\vec{r}(\psi,\zeta) - 3\vec{r}(\psi-\Delta\psi_{i-1},\zeta+\Delta\zeta) - 3\vec{r}(\psi-\Delta\psi_{i-1},\zeta) + \vec{r}(\psi-\Delta\psi_{i-1}-\Delta\psi_{i-2},\zeta+\Delta\zeta) + \vec{r}(\psi-\Delta\psi_{i-1}-\Delta\psi_{i-2},\zeta)\Big\}\Big\{46\Delta\psi_i + 4\Delta\psi_{i-1} - 2\Delta\psi_{i-2}\Big\}^{-1} \quad (4)$$

with variables as defined in Figure 2. The right-hand side of Equation 2 is computed by averaging the velocities surrounding the point $(\zeta + \Delta\zeta/2,\ \psi + \Delta\psi/2)$. The marker location is then found by substituting the difference operators and velocity averaging into Equation 2 and rearranging to obtain:

$$\vec{r}^{*m}(\psi+\Delta\psi_i,\zeta+\Delta\zeta) = \Big\{\frac{\vec{V}}{\Omega} - \Big(-\frac{1}{2\Delta\zeta}+\frac{23}{\phi}\Big)\vec{r}^{*m}(\psi+\Delta\psi_i,\zeta) - \Big(\frac{1}{2\Delta\zeta}-\frac{21}{\phi}\Big)\vec{r}^{*m}(\psi,\zeta+\Delta\zeta) + \Big(\frac{1}{2\Delta\zeta}+\frac{21}{\phi}\Big)\vec{r}^{*m}(\psi,\zeta) + \frac{3}{\phi}\vec{r}^{*m}(\psi-\Delta\psi_{i-1},\zeta+\Delta\zeta) + \frac{3}{\phi}\vec{r}^{*m}(\psi-\Delta\psi_{i-1},\zeta) - \frac{1}{\phi}\vec{r}^{*m}(\psi-\Delta\psi_{i-1}-\Delta\psi_{i-2},\zeta+\Delta\zeta) - \frac{1}{\phi}\vec{r}^{*m}(\psi-\Delta\psi_{i-1}-\Delta\psi_{i-2},\zeta)\Big\}\Big\{\frac{1}{2\Delta\zeta}+\frac{23}{\phi}\Big\}^{-1} \quad (5)$$

where

$$\vec{V} = 4V_\infty + V_{ind}\left(\vec{r}^{*m-1}(\psi,\zeta)\right) + V_{ind}\left(\vec{r}^{*m-1}(\psi+\Delta\psi,\zeta)\right) + V_{ind}\left(\vec{r}^{*m-1}(\psi,\zeta+\Delta\zeta)\right) + V_{ind}\left(\vec{r}^{*m-1}(\psi+\Delta\psi,\zeta+\Delta\zeta)\right) \quad (6)$$

$$\phi = 46\Delta\psi_i + 4\Delta\psi_{i-1} - 2\Delta\psi_{i-2} \quad (7)$$

Equation 5 is the general form of the predictor and corrector equations, indicated by the superscript m. It is first used in the predictive step to compute the predicted wake position for all Lagrangian markers using initial guess values for the wake positions ($\vec{r}^{*m}$) and velocity

values at wake positions from the previous time step ($\vec{r}^{m-1}$). The resulting wake positions are then used as the m time step in the corrector equation to compute the corrected wake position at the current time step ($\vec{r}^{m+1}$). This process iterates until converged wake locations are reached. Wake location is assumed to be converged when the difference in wake position between iterations reaches a value of less than 0.001 m Root Mean Square (RMS) [13]. This is typically achieved in two to three iterations.

The velocity term on the right-hand side of Equation 2 is a nonlinear function of the vortex position, representing a combination of the freestream and induced velocities [9]. The induced velocities at point k, caused by each straight-line filament, are computed using the Biot-Savart law, which considers the locations of the Lagrangian markers and the intensity of the vortex elements [15]:

$$d\vec{V_k} = F_\nu \frac{\Gamma}{4\pi} \frac{d\vec{l} \times \vec{r}}{|\vec{r}|^3} \tag{8}$$

Here, Γ is the circulation strength of the filament, $\vec{l}$ is the vector connecting the filament endpoint locations, and $\vec{r}$ is the perpendicular distance between $\vec{l}$ and point k. The factor F_ν is introduced because of the singularity that occurs in Equation 8 at the filament location [24]. Viscous effects prevent this singularity from occurring and diffuse the vortex strength with time. The circular zone where the velocity drops to zero around the vortex is referred to as the vortex core. An increase of length of the vortex segment will result in a decrease of the vortex core radius, and conversely for a decrease of length. Diffusion, on the other hand, continually spreads the vortex radially. To account for these effects, a viscous-core correction, F_ν, is needed. Several viscous-core models have been developed [17, 20, 24]. At present, this work uses the Vatistas model [24], defined in Equation 9.

$$F_\nu = \frac{|\vec{r}|^2}{(|\vec{r}|^{2n} + r_c^{2n})^{1/n}} \tag{9}$$

Here, n is the distance from a vortex segment to an arbitrary point [1] and r_c is the viscous core radius of a vortex filament. Research from rotorcraft applications suggests a value of $n = 2$, which is used in this work [3].

At present, the circulation along the blade span is computed using a Weissinger-L [26]-based representation of the lifting surface [7, 4, 18] and is coupled to the wake through dependence on the induced velocities. Other methods of circulation computation, such as the one from van Garrel [23], will be considered in the future. In lifting line theory, bound circulation, Γ_b, is placed on the blade at 1/4-chord and collocation points at 3/4-chord, at which a flow tangency condition is enforced. The blade is discretized into a finite number of segments, and a horseshoe vortex is used at each segment to compute the bound and trailed circulation. Note that the Weissinger-L approach is valid only for near-wake calculations. Once the circulation on the blade is determined, the circulation of the tip vortices currently being emitted is set to the maximum bound circulation. In future versions of the code, the tip vortex circulation may be set as the integral of the trailed vorticity, preserving the 0^{th} and 1^{st} moment of vorticity. At the end of a time step, the circulation of each vortex element is propagated downstream so that vortex elements with a new intensity can be emitted from the blade at the next time step.

2.2. Integration with OpenFAST

The FVW code has been integrated into the latest version of OpenFAST. Considering ease of implementation, the FVW code has been temporarily integrated with the older aerodynamic module of OpenFAST, *AeroDyn14*. The data workflow between the different modules and submodules of OpenFAST is illustrated in Figure 3. The symbols are defined as follows:

- $\vec{x}_{\text{elast},ll}$ – vector representing the position ($\vec{r}_{ll}$), orientation (Λ_{ll}), translational velocity ($\vec{\dot{r}}_{ll}$), and rotational velocity ($\vec{\omega}_{ll}$) of the different nodes of the lifting lines

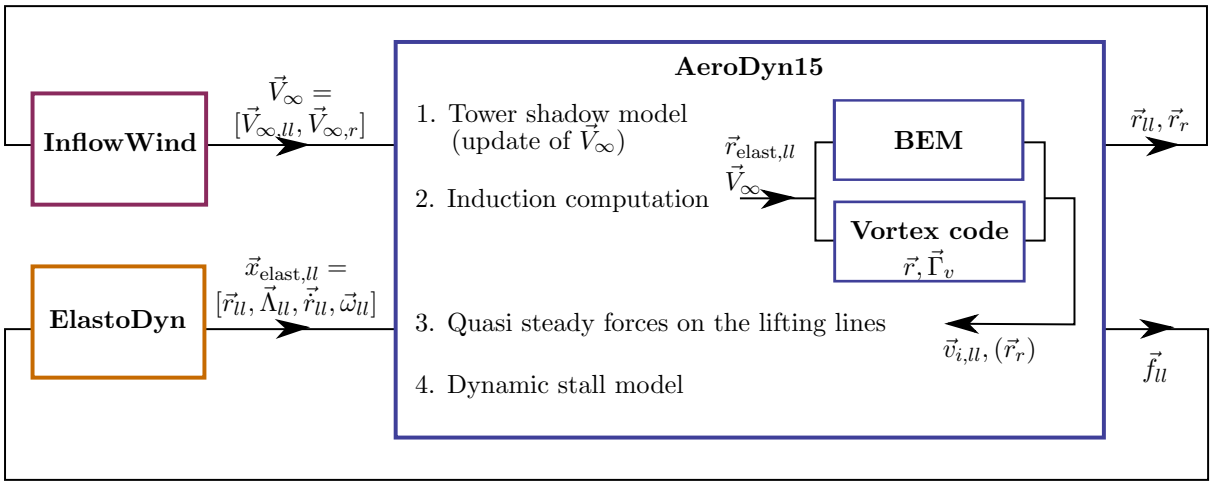

Figure 3. OpenFAST-FVW code integration workflow

- $\vec{v}_{i,ll}$ – induced velocity at the lifting line nodes, as returned by either the vortex code or the BEM code
- $\vec{f}_{ll}$ – loads at the lifting-line nodes; main output from the *AeroDyn*
- $\vec{r}_r$ – positions where the velocity is requested (typically the end points of the vortex filaments).

This integration required a restructuring of the *AeroDyn15* module to isolate the parts of the code related to tower shadow modeling, induction computation, lifting-line forces computations, and dynamic stall. The dynamic stall model will be adapted when used in conjunction with the vortex code to ensure the effect of shed vorticity is not accounted for twice. The points requested by *AeroDyn15* to the inflow module *InflowWind* to obtain the undisturbed velocity at given locations of the domain will be accommodated to potentially include the additionally requested points $\vec{r}_r$ from the vortex code, in addition to the lifting line points $\vec{r}_{ll}$. With this implementation, structural degrees of freedom will be available, allowing for analysis of highly flexible turbine blades.

3. Modeling Cases

Comparison of the developing FVW capability of OpenFAST is performed using the Big Adaptive Rotor (BAR) turbine. Note that this was developed to be a highly flexible turbine, but the current implementation of the code requires the turbine to be modeled rigidly. This newly developed three-bladed turbine model was designed as a baseline turbine for the BAR project, a U.S. Department of Energy-funded project intended to ease the design of the next generation of onshore wind turbines [10]. Some characteristics of the turbine are found in Table 1.

Simulations were performed at a range of freestream velocity with steady, no-shear inflow for both studies. Quantities of interest include axial and tangential induction distributions along the blade, as well as rotor power, though none are specifically presented here.

4. Results

This section discusses preliminary results for the baseline simulation cases of the reference BAR turbine. These results serve as an initial demonstration of the OpenFAST-FVW code, though further model integration and improvements are currently underway. Preliminary comparisons of the OpenFAST-FVW code with OpenFAST-BEM results show both promising comparisons

Table 1. Main parameters of the BAR baseline wind turbine.

Parameter	Value
Rated Electrical Power	5 MW
Rotor Diameter (D)	206.4 m
Number of Blades	3
Rotor Blade Pitch	Variable (Rated: 6.3 rpm)
Rotor Speed	Variable (Rated: 8 m/s)
Tower Height	140.0 m
Max. Chord	5.3 m

as well as clear areas of improvement. Results are nearly identical above the rated wind speed of 8 m/s, as expected. At below-rated wind speeds, the OpenFAST-FVW method predicts higher average rotor power than the OpenFAST-BEM method. For a steady, unyawed turbine, these differences are expected to be much smaller than currently observed. Such differences could be because of insufficient modeling parameters for high-thrust, high-induction cases, as previously noted, or errors in code implementation. Both options are actively being investigated.

It is important to note that the accuracy of the FVW method is dependent on proper wake discretization and the extent of the near-wake region. Specifically, when the turbine is operating with a high thrust coefficient, there is rapid wake expansion. To accurately capture this expansion, a much finer wake resolution with a more extensive near-wake area is needed. Future work will include establishing simulation guidelines for these parameters in challenging conditions.

Blade span axial and tangential induction factors along the blade span, both key output variables for analyzing aerodynamic response, were studies for several freestream velocities.There was strong agreement between OpenFAST-FVW and OpenFAST-BEM results for both axial and tangential induction at higher wind speeds, though OpenFAST-FVW results showed higher induction at the blade root for all cases. At a wind speed of 6 m/s, OpenFAST-FVW method produces lower axial induction at the blade tip. These large differences in induction are likely the cause of the discrepancies in rotor power for this wind speed. The reason for such differences is currently being investigated.

5. Conclusions and Discussion

A FVW method has been integrated into the aerodynamic module, *AeroDyn14*, within OpenFAST. Preliminary OpenFAST-FVW results using the baseline BAR turbines have been compared to OpenFAST-BEM solutions for constant inflow as an initial code comparison. Comparisons were made for turbine rotor power, as well as blade span distributions, of axial and tangential induction. These initial comparisons have led to the identifications of a few areas that need improvement, specifically the calculation of blade circulation and establishment of modeling guidelines for high-thrust cases. Additional planned code improvements include integration into the newer module, *AeroDyn15*. In this version, the vortex code will comply with the modularization framework of OpenFAST [11, 12].

Once the code has been sufficiently developed, code verification and validation will be carried out with detailed comparisons to LES results, NREL UAE Phase IV turbine experimental measurements, and experimental blade load measurements for highly flexible rotors. Additionally, several cases known to be challenging for BEM models will be simulated for the BAR turbine and compared to the FVW results. These conditions include:

- Large cone angle (15°)
- High yaw angle (30°)

- High inflow shear (0.4)
- High turbulence, low wind speed (TI=18 %, $U_\infty = 5$ m/s)
- Highly flexible blades

The first phase of this work focuses on code implementation for single-turbine capabilities, fulfilling the basic requirements for the design of large and novel rotor concepts, such as the ones considered within the BAR project. Future development work includes enabling multiturbine simulations on medium- to large-scale computational clusters. Reduction of the computational time will also be of focus. This may be achieved using tree techniques such as the fast-multipole method. Further algorithmic options, such as vortex amalgamation in the wake, will be considered. Grid-free or grid-based vortex particle formulations, compatible with the framework presented here, will also be considered in the future. Applications to cases known to be challenging for the BEM algorithm will also be investigated (e.g., highly flexible rotors, offshore floating turbines, small-scale wind farms, multiple-rotor turbines, or kites).

Acknowledgments

This work was authored by the National Renewable Energy Laboratory, operated by Alliance for Sustainable Energy, LLC, for the U.S. Department of Energy (DOE) under Contract No. DE-AC36-08GO28308. Funding provided by the U.S. Department of Energy Office of Energy Efficiency and Renewable Energy Wind Energy Technologies Office. The views expressed in the article do not necessarily represent the views of the DOE or the U.S. Government. The U.S. Government retains and the publisher, by accepting the article for publication, acknowledges that the U.S. Government retains a nonexclusive, paid-up, irrevocable, worldwide license to publish or reproduce the published form of this work, or allow others to do so, for U.S. Government purposes.

References

[1] H. Abedi. *Development of Vortex Filament Method for Wind Power Aerodynamics*. Phd thesis, Chalmers University of Technology, Gothenburg, Sweden, 2016.

[2] S. Ananthan, J. G. Leishman, and M. Ramasamy. The role of filament stretching in the free-vortex modeling of rotor wakes. In *58th Annual Forum and Technology Display of the American Helicopter Society International*, Montreal, Canada, June 2002.

[3] A. Bagai and J. G. Leishman. Flow visualization of compressible vortex structures using density gradient techniques. *Experiments in Fluids*, 15(6):431–442, 1993.

[4] A. Bagai and J. G. Leishman. Rotor free-wake modeling using a pseudo-implicit technique—including comparisons with experimental data. In *50th Annual Forum of the American Helicopter Society*, pages 29–39, Washington, D.C., May 1994.

[5] E. Branlard. *Wind Turbine Aerodynamics and Vorticity-Based Methods: Fundamentals and Recent Applications*. Springer International Publishing, 2017.

[6] E. Branlard, G. Papadakis, M. Gaunaa, G. Winckelmans, and T. J. Larsen. Aeroelastic large eddy simulations using vortex methods: unfrozen turbulent and sheared inflow. *Journal of Physics: Conference Series (Online)*, 625, 2015.

[7] S. Gupta. *Development of a Time-Accurate Viscous Lagrangian Vortex Wake Model for Wind Turbine Applications*. Phd thesis, Univeristy of Maryland, College Park, MD, 2006.

[8] S. Gupta and J. G. Leishman. Free-vortex filament methods for the analysis of helicopter rotor wakes. *Journal of Aircraft*, 39(5):759–775, 2002.

[9] M. O. L. Hansen. *Aerodynamics of Wind Turbines*. Earthscan, London; Sterling, VA, 2008.

[10] N. Johnson, P. Bortolotti, K. Dykes, and et al. Investigation of innovative rotor concepts for the big adaptive rotor project. Technical Report NREL/TP-5000-73605, National Renewable Energy Laboratory, 2019.

[11] J. Jonkman. The new modularization framework for the fast wind turbine cae tool. Technical report NREL/CP-5000-57228, National Renewable Energy Laboratory, 2013.

[12] J. Jonkman, M. A. Sprague, and B. J. Jonkman. Fast modular framework for wind turbine simulation: New algorithms and numerical examples. Technical report NREL/CP-2C00-63203, National Renewable Energy Laboratory, 2015.

[13] K. Kecskemety. *Assessing the Influence of Wake Dynamics on the Performance and Aeroelastic Behavior of Wind Turbines*. Phd thesis, Ohio State University, Columbus, OH, 2012.
[14] J. Leishman. *Principles of Helicopter Aerodynamics*. Cambridge Univ. Press, Cambridge, MA, 2006.
[15] J. G. Leishman, M. J. Bhagwat, and A. Bagai. Free-vortex filament methods for the analysis of helicopter rotor wakes. *Journal of Aircraft*, 39(5):759–775, 2002.
[16] G. Papadakis. *Development of a hybrid compressible vortex particle method and application to external problems including helicopter flows*. PhD thesis, National Technical University of Athens, 2014.
[17] W. J. M. Rankine. *Manual of Applied Mechanics*. Griffen Co., London, 1858.
[18] M. Ribera. *Helicopter Flight Dynamics Simulation with a Time-Accurate Free-Vortex Wake Model*. Phd thesis, University of Maryland, College Park, MD, 2007.
[19] L. Rosenhead. The formation of vortices from a surface of discontinuity. *Proceedings of the Royal Society of London. Series A, Containing Papers of a Mathematical and Physical Character*, 134(823):170–192, 1931.
[20] M. P. Scully. *Computation of Helicopter Rotor Wake Geometry and Its Influence on Rotor Harmonic Airloads*. Phd thesis, Massachusetts Institute of Technology, Cambridga, MA, 1975.
[21] M. Sessarego, N. Ramos García, J. N. Sørensen, and W. Z. Shen. Development of an aeroelastic code based on three-dimensional viscous-inviscid method for wind turbine computations. *Wind Energy*, 20(7):1145–1170, 2017.
[22] K. Shaler. *Wake Interaction Modeling Using A Parallelized Free Vortex Wake Model*. Phd thesis, Ohio State University, Columbus, OH, 2020.
[23] A. van Garrel. Development of a wind turbine aerodynamics simulation module. Technical Report ECN-C–03-079, ECN, 2003.
[24] G. H. Vatistas, V. Koezel, and W. C. Mih. A simpler model for concentrated vortices. *Experiments in Fluids*, 11(1):73–76, 1991.
[25] S. G. Voutsinas. Vortex methods in aeronautics: how to make things work. *International Journal of Computational Fluid Dynamics*, 2006.
[26] J. Weissinger. The lift distribution of swept-back wings. Technical report TM 1120, NACA, 1947.
[27] G. S. Winckelmans and A. Leonard. Contributions to vortex particle methods for the computation of 3-dimensional incompressible unsteady flows. *Journal Of Computational Physics*, 109(2):247–273, 1993.
[28] R. Wiser and M. Bolinger. 2016 wind technologies market report. Technical Report DOE/GO-102917-5033, Lawrence Berkeley National Laboratory, Berkeley, CA, August 2017.